Antigenic and virological characteristics of SARS-CoV-2 variants BA.3.2, XFG, and NB.1.8.1

The SARS-CoV-2 saltation variant BA.3.2, harbouring over 50 mutations relative to its ancestral BA.3 lineage, has recently drawn global attention (figure A). Notably, BA.3.2 exhibits 44 mutations distinct from the currently dominant LP.8.1/LP.8.1.1 variant (appendix p 4), raising speculation about its potential to drive an outbreak similar to BA.2.86/JN.1, particularly following its first detection outside South Africa in the Netherlands on April 2, 2025.[1–5] A critical evaluation of its antigenic profile and infectivity is essential to establish its likelihood of prevailing.

Concurrently, multiple emerging variants—including NB.1.8.1, LF.7.9, XEC.25.1, XFH, and XFG—exhibit enhanced growth advantages over LP.8.1.1, which suggests their potential to dominate future transmission waves (figure B). These variants show convergent evolution of recurrent mutations such as Gln493Glu, Ala435Ser, and Ala475Val (figure A).[6–8] Specifically, NB.1.8 and NB.1.8.1, descendants of the XDV.1.5.1 sublineage, are characterised by Gln493Glu and Ala435Ser mutations, respectively, and have rapidly spread in China and Hong Kong. Similarly, XEC.25.1, a derivative of XEC, harbours the Ala435Ser mutation and also shows a high growth advantage. LF.7.9, a highly fit European variant derived from LF.7, carries the receptor-binding domain (RBD) mutations Ala475Val, Leu441Arg, and His445Pro. The recombinant

Lancet Infect Dis 2024
Published Online
June 5, 2025
https://doi.org/10.1016/S1473-3099(25)00308-1

See Online for appendix

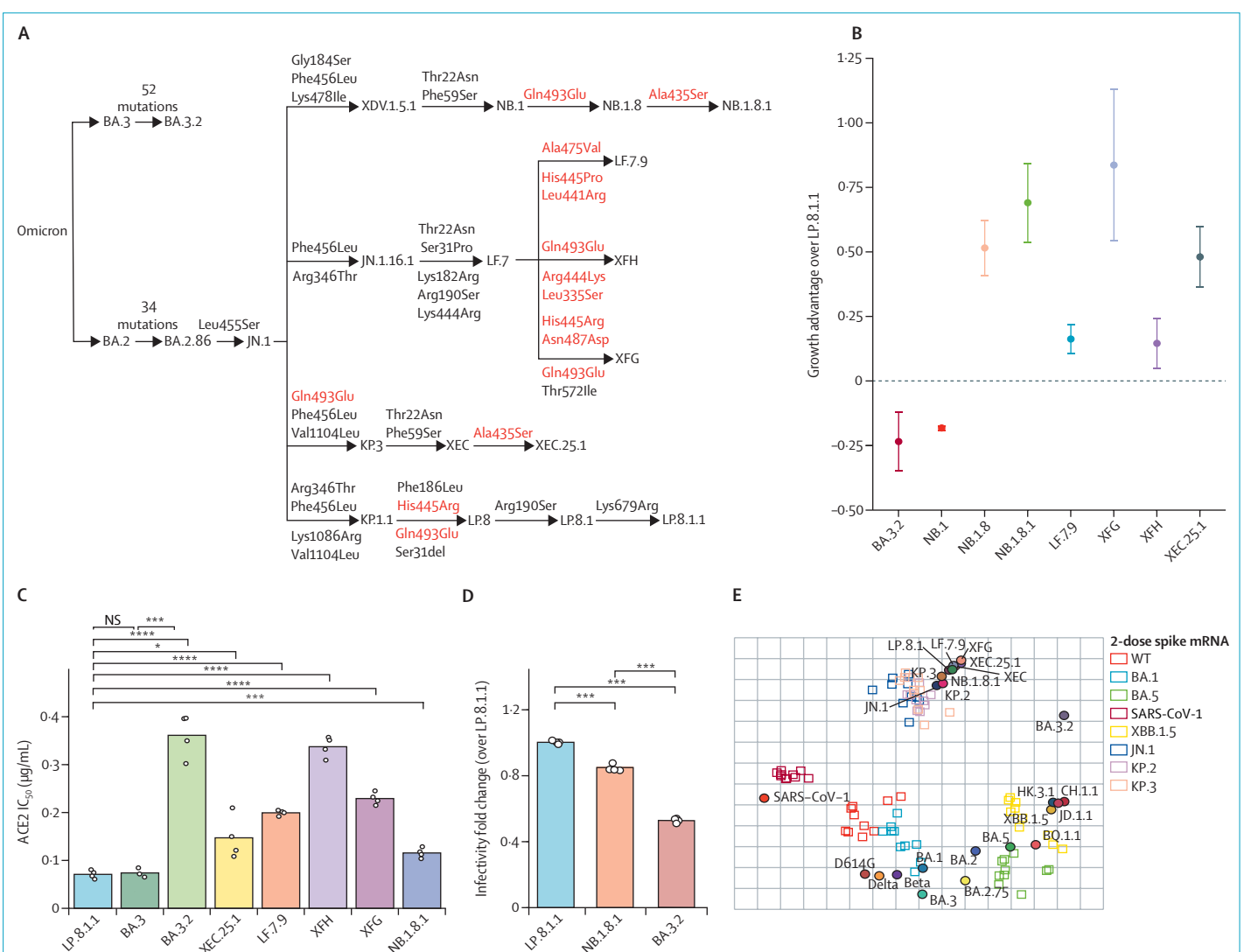

(Figure continues on next page)

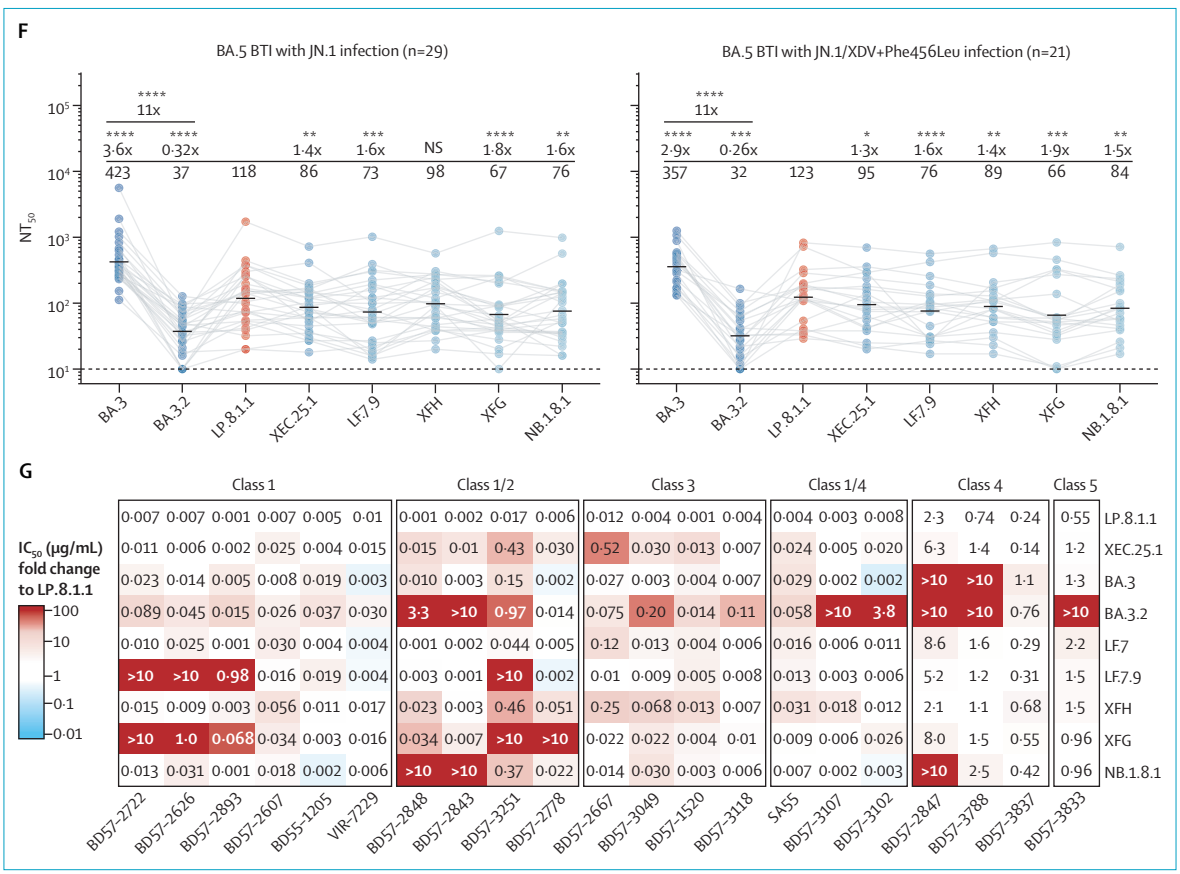

Figure: **Antigenic and virological characteristics of emerging SARS-CoV-2 variants BA.3.2, XFG, and NB.1.8.1**
(A) Genetic changes in the spike glycoprotein of prevalent SARS-CoV-2 variants; key mutations observed in these variants are marked in red. (B) The relative growth advantage of BA.3.2, NB.1, NB.1.8, NB.1.8.1, LF.7.9, XFG, XFH, and XEC.25.1 compared with LP.8.1.1. Daily global sequence data retrieved from the Global Initiative on Sharing All Influenza Data database (April 1, 2024–April 11, 2025) were used to compute the relative growth advantage. Growth advantage was calculated with the generation time set to 7 days, and CIs were calculated with α=0·95. (C) IC_{50} values for the neutralisation of LP.8.1.1, BA.3, BA.3.2, XEC.25.1, LF.7.9, XFH, XFG, and NB.1.8.1 pseudoviruses by soluble human ACE2. Technical replicates are shown as individual circles. IC_{50} (μg/mL) was log-transformed before two-tailed *t* test analysis. (D) Relative infectivity of NB.1.8.1 and BA.3.2 compared with LP.8.1.1 in Vero cells. Infectivity was assessed by use of vesicular stomatitis virus pseudoviruses. Each dot represents a replicate and bars denote mean values. Significance was evaluated by use of a two-tailed *t* test. (E) Antigenic map based on NT_{50} titres from plasma of mice immunised with two doses of spike mRNA vaccines against indicated strains. The map was generated by use of modified multidimensional scaling in Racmacs (version 1.1.35) and visualized with ggplot2 (version 3.4.1) after 500 optimisation steps with the minimum column basis set to none. (F) NT_{50} values were measured from convalescent plasma of individuals reinfected with JN.1 post-BA.5/BF.7 BTI (n=29), or with JN.1/XDV (Phe456Leu) post-BA.5/BF.7 (n=21). Cohort labels and sample sizes are provided above each panel. The dashed line represents the detection limit (NT_{50}=10). Geometric means, fold reductions, and corresponding p values (Wilcoxon rank-sum test) are noted above each group. (G) IC_{50} values (μg/mL) of monoclonal neutralising antibodies targeting RBD epitopes against BA.3, BA.3.2, LP.8.1.1, XEC.25.1, LF.7.9, XFH, XFG, and NB.1.8.1 variants. Fold changes relative to LP.8.1.1 are shown by background colour: red denotes increased resistance and blue denotes enhanced sensitivity. Colour scale indicates the fold-change magnitude. BTI=breakthrough infection. IC_{50}=50% inhibitory concentration. NS=not significant. NT_{50}=50% neutralisation titre. RBD=receptor-binding domain. WT=wildtype; Wuhan-Hu-1 reference strain. *p<0·05. **p<0·01. ***p<0·001. ****p<0·0001.

XFG variant, originating from LF.7 and LP.8.1.2, harbours four key spike mutations (His445Arg, Asn487Asp, Gln493Glu, and Thr572Ile) and has achieved rapid global spread following its initial detection in Canada. Another recombinant variant, XFH, originating from LF.7.1 and XEF, carries the convergent mutation Gln493Glu, a reversion of Arg444Lys, and a novel Leu335Ser mutation, also positioning it among the fastest-growing variants to date. The concurrent emergence of BA.3.2 alongside these variants necessitates urgent comparative analysis of their antigenic and virological characteristics to evaluate whether BA.3.2 can outcompete existing lineages.

First, we generated spike-pseudotyped vesicular stomatitis viruses for the concerning variants and assayed the efficiency of soluble human angiotensin-converting enzyme 2 (hACE2) to inhibit viral entry, which reflects the ACE2-binding strength and receptor engagement efficiency of each variant's spike protein (figure C). Recombinant RBD subunits were also produced, and their binding affinity to hACE2 was quantified via surface plasmon resonance (appendix p 5). Surprisingly, all tested variants exhibited relatively lower ACE2-binding capability compared with LP.8.1.1. Specifically,

BA.3.2's spike exhibited the lowest ACE2 engagement efficiency, which was significantly reduced compared with its ancestor BA.3 and LP.8.1.1. However, BA.3.2's RBD actually displayed similar ACE2-binding affinity to LP.8.1.1, suggesting that its reduced spike-mediated ACE2 engagement arises from a relatively closed spike or down RBD conformation. Similarly, XFH exhibited low ACE2 engagement efficiency, probably due to a closed spike conformation induced by the Leu335Ser mutation. In contrast, LF.7.9 and XFG showed markedly reduced RBD–ACE2 binding affinity, attributable to their Ala475Val and Asn487Asp mutations, respectively, which explain their lower receptor engagement efficiency. Notably, XEC.25.1 and NB.1.8.1 retained robust ACE2 engagement, with NB.1.8.1 exhibiting the highest RBD–ACE2 binding affinity among all variants tested. Consistent with these findings, pseudovirus infectivity assayed in Vero cells revealed that BA.3.2 exhibits disastrously low fitness compared with LP.8.1.1, whereas NB.1.8.1 retains acceptable infectivity (figure D).

Next, we evaluated the antigenicity and humoral immune evasion properties of these variants using pseudovirus neutralisation assays. Antigenicity was assessed by use of serum samples from naive mice immunised with two doses of spike mRNA vaccines, whereas antibody evasion capability was tested with human convalescent plasma. The plasma used in this study was obtained from two cohorts of individuals who received two or three doses of inactivated SARS-CoV-2 vaccines and subsequently had BA.5 or BF.7 breakthrough infection, with one cohort reinfected by JN.1 (n=29) and the other by JN.1 or XDV with Phe456Leu (n=21), as previously described (appendix p 13).[3] Notably, BA.3.2 exhibited high resistance to serum neutralisation across all naive mouse vaccine groups (appendix p 6). Antigenic cartography based on pseudovirus neutralisation titres revealed BA.3.2 to be antigenically distinct from the JN.1 and XBB.1.5 lineages, whereas LF.7.9, XEC.25.1, XFG, and NB.1.8.1 all clustered close to the JN.1 family (figure E).[8] In human plasma, BA.3.2 also showed profound humoral immune evasion, with an 11-fold reduction in geometric mean 50% neutralisation titre (NT_{50}) compared with BA.3 and a 3–4-fold reduction relative to LP.8.1.1 (figure F). Although BA.3.2 showed the strongest evasion, XFG, LF.7.9, and NB.1.8.1 also displayed enhanced escape compared with LP.8.1.1 in both cohorts: XFG exhibited a nearly 2-fold decrease in NT_{50}, whereas LF.7.9 and NB.1.8.1 showed 1·5–1·6-fold reductions, consistent with their relative growth advantages over LP.8.1.1 (figure F).

To delineate the molecular basis of immune evasion, we profiled the sensitivity of these variants to a panel of RBD-targeting neutralising monoclonal antibodies spanning distinct epitopes (figure G and appendix p 7). LF.7.9 exhibited pronounced resistance to class 1 antibodies, primarily driven by its Ala475Val mutation, whereas XFG resistance was attributed to its Asn487Asp and Gln493Glu mutations. The Asn487Asp mutation in XFG additionally conferred escape from class 1/2 (group B) antibodies.[8] Similarly, the Lys478Ile mutation in NB.1.8.1 and Lys478Asn in BA.3.2 enhanced the evasion of class 1/2 antibodies. The Ala435Ser mutations in XEC.25.1 and NB.1.8.1 reduced antibody neutralisation potency across all epitopes, similar to observations in MC.10.1.[3] Strikingly, BA.3.2 showed robust escape from class 1/4 antibodies, a class of potent, broad-spectrum neutralising antibodies effective against most omicron lineages, including LF.7.9, XEC.25.1, XFG, XFH, and NB.1.8.1 (figure G). Notably, class 1/4 antibodies are prevalent in Chinese populations immunised with inactivated vaccines, where immune imprinting is less pronounced.[9,10] In contrast, mRNA vaccine recipients with stronger immune imprinting rarely develop these antibodies, which might cause divergent neutralisation responses against BA.3.2 between these groups.

In summary, our findings indicate that BA.3.2 exhibits robust antibody evasion but has low ACE2-binding capability and infectivity, which substantially limits its likelihood of prevailing. To achieve efficient spread akin to BA.2.86 or JN.1, BA.3.2 would require additional mutations to improve both its receptor engagement efficiency (eg, stabilising an open RBD conformation) and its evasion of class 1 antibodies. Similarly, although XFG displays strong immune evasion, its relatively low ACE2 engagement efficiency suggests that it might need compensatory mutations to enhance receptor compatibility for sustained transmission. Importantly, NB.1.8.1 shows a balanced profile of ACE2 binding and immune evasion, supporting its potential for future prevalence.

CG and YY contributed equally. YC has provisional patent applications for the BD series antibodies (WO2024131775A9 and WO2023151312A1), and is the founder of Singlomics Biopharmaceuticals. All other authors declare no competing interests.

*Caiwan Guo, Yuanling Yu, Jingyi Liu, Fanchong Jian, Sijie Yang, Weiliang Song, Lingling Yu, Fei Shao, *Yunlong Cao*

yunlongcao@pku.edu.cn

Biomedical Pioneering Innovation Center (BIOPIC), Peking University, Beijing, China (CG, JL, FJ, SY, WS, YC); Changping Laboratory, Beijing, China (CG, YY, JL, FJ, SY, WS, LY, FS, YC); Academy for Advanced Interdisciplinary Studies, Peking University, Beijing, China (CG); College of Future Technology, Peking University, Beijing, China (JL); College of Chemistry and Molecular Engineering, Peking University, Beijing, China (FJ); Peking-Tsinghua Center for Life Sciences, Tsinghua University, Beijing, China (SY, YC); School of Life Sciences, Peking University, Beijing, China (WS, YC)

1 Zhang L, Kempf A, Nehlmeier I, et al. Host cell entry and neutralisation sensitivity of the emerging SARS-CoV-2 variant LP.8.1. *Lancet Infect Dis* 2025; **25:** e196–97.

2 Chen L, Kaku Y, Okumura K, et al, and the Genotype to Phenotype Japan (G2P-Japan) Consortium. Virological characteristics of the SARS-CoV-2 LP.8.1 variant. *Lancet Infect Dis* 2025; **25:** e193.

3 Liu J, Yu Y, Yang S, et al. Virological and antigenic characteristics of SARS-CoV-2 variants LF.7.2.1, NP.1, and LP.8.1. *Lancet Infect Dis* 2025; **25:** e128–30.

4 Yang S, Yu Y, Xu Y, et al. Fast evolution of SARS-CoV-2 BA.2.86 to JN.1 under heavy immune pressure. *Lancet Infect Dis* 2024; **24:** e70–72.

5 Yang S, Yu Y, Jian F, et al. Antigenicity and infectivity characterisation of SARS-CoV-2 BA.2.86. *Lancet Infect Dis* 2023; **23:** e457–59.

6 Liu J, Yu Y, Jian F, et al. Enhanced immune evasion of SARS-CoV-2 variants KP.3.1.1 and XEC through N-terminal domain mutations. *Lancet Infect Dis* 2025; **25:** e6–e7.

7 Kaku Y, Okumura K, Kawakubo S, et al, and the Genotype to Phenotype Japan (G2P-Japan) Consortium. Virological characteristics of the SARS-CoV-2 XEC variant. *Lancet Infect Dis* 2024; **24:** e736.

8 Jian F, Wang J, Yisimayi A, et al. Evolving antibody response to SARS-CoV-2 antigenic shift from XBB to JN.1. *Nature* 2025; **637:** 921–29.

9 Cao Y, Jian F, Wang J, et al. Imprinted SARS-CoV-2 humoral immunity induces convergent omicron RBD evolution. *Nature* 2023; **614:** 521–29.

10 Yisimayi A, Song W, Wang J, et al. Repeated omicron exposures override ancestral SARS-CoV-2 immune imprinting. *Nature* 2024; **625:** 148–56.